Polarization Reversal of Low Frequency Magnetic Variation in the Lunar Wake

Tomoko Nakagawa[1], Futoshi Takahashi[2], Yoshifumi Saito[3], and Hisayoshi Shimizu[4]

[1]Department of Information and Communication Engineering, Tohoku Institute of Technology, Miyagi, 982-8577 Japan.

[2]Department of Earth and Planetary Sciences, Faculty of Science, Kyushu University, Fukuoka 819-0395.

[3]Institute of Space and Astronautical Science, Japan Aerospace Exploration Agency, Kanagawa, 229-8510 Japan.

[4]Earthquake Research Institute, University of Tokyo, Tokyo 113-0032, Japan.

Corresponding author: Tomoko Nakagawa (nakagawa@tohtech.ac.jp)

Key Points:

- Kaguya detected unified polarization of the magnetic field variation in a frequency range from 0.01 to 0.3 Hz in the lunar wake.
- The sense of rotation of magnetic field reversed at the equator under the condition of dawn-dusk directed magnetic field.
- The magnetic field variation was perpendicular to the background magnetic field and can penetrate into the deepest wake.

Abstract

Reversal of unified polarization of low-frequency magnetic field variation was found by Kaguya at equator crossings in the lunar wake under the condition of dawn-dusk directed background magnetic field. The polarization was left-handed over a frequency range from 0.01 to 0.3 Hz in the southern hemisphere of the lunar wake in the dawnward-directed magnetic field. It turned to be right-handed when the spacecraft entered the northern hemisphere of the wake. In the duskward-directed magnetic field the polarization reversed. The same configuration by 90 degrees rotated was observed in northward-directed magnetic field, too. The sense of rotation was alike that of surface waves generated by Kelvin-Helmhlotz instability, but it was not likely because the waves of unified polarization were not always accompanied by velocity shear. They penetrated into the very center of the wake, suggesting that they were not propagating along a surface of wake boundary. The polarization was highly elliptic except for high frequency component. The magnetic field variation was predominantly perpendicular to the background magnetic field, suggesting that they were shear Alfven waves. The mechanism of unifying the polarization is not yet understood.

Plain Language Summary

The moon is exposed to the supersonic flow of the solar wind. The lunar surface absorbs most of the solar wind particles, leaving a void region called a lunar wake. There is no direct bombardment of solar wind ions on the nightside surface of the moon, and magnetic field fluctuation is weaker in the wake than in the dayside solar wind. Kaguya spacecraft on its polar orbit observed the magnetic field variation in the wake, and found clear reversal of direction of rotation of the magnetic variation at its equator crossing under the condition of dawn-dusk directed background magnetic field. No such rotation has not been found in plasma flow.

1 Introduction

The moon is exposed to the solar wind flow for most of the time in its orbit, and bombarded by the solar wind particles due to the lack of global scale magnetic field or dense atmosphere. The lunar surface absorbs most of the incident solar wind particles, leaving a plasma cavity called the lunar wake behind the moon (Schubert and Lichtenstein, 1974, and references therein). Loss of solar wind particles was observed by Explorer 35 in the umbra of the moon (Lyon et al., 1967), and quantitative assessment of reduction of plasma density in the wake down to two orders of unperturbed solar wind was revealed by WIND at 6.5 lunar radii downstream of the moon (Bosqued et al., 1996). WIND also detected counter streaming cold ion beams refilling the plasma void (Ogilvie et al., 1996). Magnetic field fluctuations were also regarded as signatures of the lunar wake. Enhancement of the magnetic field were observed in the umbra together with dips at the lunar wake boundary (Colburn et al., 1967; Ness et al., 1968).

Wake-related waves in the magnetic field have been reported since the very early years of spaceborne observation, but most of them were detected out of the wake on field lines connected to the lunar wake but not in the center of the wake (Ness and Schatten, 1969; Krall and Tidman, 1969). Farrell et al. (1996) found whistler mode waves detected in the solar wind on field lines connected to the wake, and attributed them to the counter-streaming electrons reflected at the wake boundary. Bale et al. (1997) reported ion acoustic waves and

Langmuir waves on field lines connected to the wake, but again not in the very center of the wake.

The magnetic field in the center of the lunar wake is essentially quiet (Harada et al., 2015) due to the absence of solar wind injection, with only a few exceptions of for ELF waves associated with "type-II entry protons" (Nakagawa et al., 2015; Nishino et al., 2009, 2010, 2013). It makes a clear contrast to the enhanced wave activity on dayside of the moon, where backscattered or reflected plasma particles (Saito et al., 2008, 2010, 2012; McComas et al., 2009; Wieser et al., 2009, 2011; Lue et al., 2011; Poppe et al., 2014) generate a various type of wave activities (Harada and Halekas, 2016 and references therein; Halekas et al., 2006; Nakagawa et al., 2011, 2012; Tsugawa et al., 2011, 2012; Nakagawa, 2016),

Although the power density is low, uniform sense of rotation has been found in low-frequency fluctuations of magnetic field in each hemisphere in the lunar wake, depending on the direction of the background magnetic field. This paper reports the nature of the polarization of the low frequency magnetic fluctuations in the lunar wake.

2 Data and Methods

The magnetic field and the plasma momentum data used in this study were obtained by Magnetic field and Plasma experiment (MAP) onboard Kaguya spacecraft (Kato et al., 2010). The spacecraft was on its polar orbit encircling the moon at an altitude of 100 km – 80 km. Figure 1 (a)-(d) show an example of the orbit of Kaguya together with the moon on 30 March 2008.

The Lunar MAGnetometer (MAP-LMAG) obtained the magnetic field vectors with sampling frequency of 32 Hz (Shimizu et al.,2008; Takahashi et al., 2009; Tsunakawa et al., 2010). The 1s averages of the MAP-LMAG data were Fourier transformed every 120 s sliding a Humming window by 60 s. Minimum variance analysis (Sonnerup and Cahill, 1967) was applied to each Fourier component, and the components were coordinate transformed into the minimum, intermediate and maximum variance directions. The Fourier component in intermediate and maximum directions were separated into left-handed or right-handed polarization with respect to the background magnetic field. The sense of polarization Q is defined as

$$Q = \frac{b_L^2 - b_R^2}{b_L^2 + b_R^2},$$

where b_L and b_R are amplitudes of the left-hand or right-hand polarized waves that compose each Fourier component, respectively. The ellipticity is defined by the ratio of the length of the semi-minor axis to the length of the semi-major axis of the polarization ellipse of each Fourier component. In minimum variance coordinates, the ellipticity corresponds to the ratio of the amplitudes of intermediate to maximum variance. Coherence coh_{xy}, coh_{yz}, and coh_{zx} between two of the 3 components of magnetic field fluctuations were calculated from the averages of cross spectra and power spectra of 4 sets of 120-s spectra shifted by 30 s according to Fowler et al. (1967) as

$$coh_{xy} = \frac{\sqrt{< K_{xy} >^2 + < J_{xy} >^2}}{\sqrt{< S_{xx} >^2}\sqrt{< S_{yy} >^2}},$$

where $< K_{xy}(\omega) >$ and $< J_{xy}(\omega) >$ are averages of cospectrum $K_{xy}(\omega) = a_x(\omega)a_y(\omega) + b_x(\omega)b_y(\omega)$ and quadspectrum $J_{xy}(\omega) = a_x(\omega)b_y(\omega) - b_x(\omega)a_y(\omega)$, respectively, while $< S_{xx}(\omega) >$ and $< S_{yy}(\omega) >$ are averages of power spectra $S_{xx}(\omega) = a_x(\omega)^2 + b_x(\omega)^2$ and $S_{yy}(\omega) = a_y(\omega)^2 + b_y(\omega)^2$. Here $a_x(\omega)$, $b_x(\omega)$, and $a_y(\omega)$, $b_y(\omega)$ are Fourier components of time series of magnetic field components $B_x(t)$ and $B_y(t)$.

The Plasma energy Angle and Composition Experiment (MAP-PACE) made 3-dimensional plasma measurements with 4 sensors, IMA (Ion Mass Analyzer), IEA (Ion Energy Analyzer), ESA (Electron Spectrum Analyzer)-1 and ESA-2 (Saito et al., 2010). IMA and IEA obtained 3-dimensional velocity distribution function of low-energy ions below 29keV/q within 1 s, while ESA-1 and ESA-2 were for low-energy electrons below 16keV in 1 s. The IMA and ESA-1 sensor were installed on the nadir-looking panel of the spacecraft, while the IEA and ESA-2 sensors were on the zenith-looking panel (Saito et al., 2010). Each distribution function was integrated to obtain momentum data, and the results from IMA and IEA were combined to obtain ion density and ion bulk velocity. Temporal resolution of the final momentum varies from 1 s to 16 s depending on operation mode. Electron density and bulk velocity were calculated in the same way from ESA-1 and ESA-2 momentum data.

Upstream solar wind plasma and magnetic field condition was monitored by using Level 2 data from the Solar Wind Electron, Proton, and Alpha Monitor (SWEPAM) and the Magnetic Field Experiment (MAG) onboard the Advanced Composition Explorer (ACE) spacecraft.

3 Results

3.1 Polarization reversal of magnetic field variation at equator crossing

Figure 1 shows an example of dynamic spectra of the magnetic field variation in the lunar wake observed on 30 March, 2008. Top panels show the position of the spacecraft in (a) Geocentric Solar Ecliptic (GSE) coordinates, (b) (c) Selenocentric Solar Ecliptic (SSE) coordinates and (d) Mean Earth polar axis (ME) coordinates. The moon was in the solar wind and the spacecraft was in a polar orbit in noon-midnight meridian passing through the wake from the southern side to the northern side. The solar wind was stable during the Kaguya passage through the wake. The upstream ion number density was about $2 \times 10^6\ \mathrm{m}^{-3}$ and the bulk speed was 498 km/s according to ACE observation made at 1.53×10^6 km in the solar wind upstream of the moon and time-shifted by about 50 min for the solar wind flow to travel the distance.

In Figure 1(e) the lunar wake is recognized by the drop of electron density (the gray curve) by 10^{-2} times. The red curve is the sum of ion densities obtained by IMA and IEA sensors. As the spacecraft proceeded to the nightside of the moon, the IEA density (pink curve) decreased and only the IMA density (orange curve) became available. The decrease of ions was consistent with that of electrons. The density gradient was sharp and the ion number density decreased one-order (1/10) within 56 km in Z_{sse} direction in both hemispheres (6:55:00-6:56:19 and 7:40:00-7:42:06).

Outside the wake (6:00–6:54 and 7:41–8:00), the power density of the magnetic field variation was higher than inside, and there was no preferred polarization. As the spacecraft entered into the southern hemisphere of the lunar wake at 6:54, the polarization turned to be left-handed (blue in Figure 1 (g)) with respect to the background magnetic field. After the

crossing of the equator at 7:18, the polarization turned to be right-handed (red) in the northern hemisphere and persisted until the spacecraft exit the wake at 7:42. The background magnetic field was nearly dawnward (negative B_y in Figure 1 (k)) during the passage through the wake.

Significance of the polarization is examined in Figure 2 which shows coherence between each components of the magnetic field. Clear coherence was observed only between B_z and B_x. This is consistent with magnetic field rotation around the background magnetic field in Y_{sse} direction.

The sense of rotation of the magnetic field variation with respect to the dawnward-directed background field is illustrated in Figure 3(a). Both the left-hand polarization in the southern hemisphere and the right-hand polarization in the northern hemisphere is consistent with the flow direction of vortices behind an obstacle in a fast flow.

Figure 4 shows examples of power density spectra and waveforms adapted from the period in Figure 1, (a) 7:04 –7:06 and (b) 7:06–7:08 in the southern hemisphere, (c) 7:19–7:21 around the equator, and (d) 7:38–7:40 and (e) 7:41–7:43 in the northern hemisphere. In the left panels, the peak frequency was well below the proton cyclotron frequency. Thus, the waves are supposed to be essentially magnetohydrodynamic. It should be noted that there were high frequency components above the cyclotron frequency in panels (a), (d) and (e).

The right panels of Figure 4 show the waveforms. The amplitudes were of the order of 1 nT or more. The amplitude was not depressed in panel (c), indicating that the wave penetrated deep into the very center of the wake far from the wake boundary. Magnitude of the magnetic field as well as the components were variable, indicating that the waves were compressional.

Figure 5 shows hodograms of the paths of the tips of the magnetic vectors for the same 120-s periods in Figure 4. In each panel, the beginning of the period was marked with a red small circle. The right panels show traces in a plane of intermediate and maximum variance, with normal component of the background magnetic field out of the plane toward the reader. Panel (a) shows left-hand polarization with respect to the background magnetic field, while panels (c), (d), and (e) exhibit right-handed polarization. Panel (b) shows mixture of left-handed and right-handed polarizations.

Although the sense of rotation can be recognized in Figure 5, the polarization was highly elliptic. Figure 1(h) shows ellipticity, which is equivalent to the ratio of amplitudes in intermediate and maximum variance directions. In the wake, the ellipticity was close to 0 indicating that the waves were nearly linearly polarized. Only exceptions are high frequency component above 0.2 Hz at around 07:01 and 07:38 whose polarization was circular.

Figure 1(i) shows the angle between the **k** vector (the minimum variance direction) and the background magnetic field. Compared with those outside of the wake, the angle was smaller in the wake. The high frequency components above 0.2 Hz had **k** vectors nearly parallel to the background magnetic field.

Figure 6 shows bulk velocity as well as plasma density obtained by MAP/PACE onboard Kaguya for the same period as Figure 1, 06:00 –08:00 on 30 March, 2008. The ion velocity obtained by IEA (pink curves) and IMA (orange curves) are combined to obtain the bulk velocity (red curves). Outside the wake, the bulk speed was 500 km/s, consistently with the upstream solar wind observation by ACE. Downstream of the terminator, only the IMA velocity (orange curves) was available. On the northern wake boundary at around 7:40, a

gradual depression of the velocity component $|V_x|$ in the wake boundary was recognized while no such gradient was seen in the southern wake boundary at around 6:55. Figure 6 also has gray curves of electron bulk velocity, but in general it is difficult to obtain accurate bulk velocity of electrons because it is calculated from small shift of wide-spread velocity distribution.

3.2 Polarization reversal in duskward IMF

Figure 7 shows another example of polarity reversal observed in the duskward-directed magnetic field on 7 April 2008. The upstream solar wind condition was 3.5×10^6 m^{-3} of ion density and 614 km/s in bulk velocity according to ACE observation. The orbit of Kaguya was again in noon-midnight meridian. Contrary to Figure 1, the polarization was right-handed in the southern wake and turned to be left-handed in the northern wake at the equator crossing at 19:32. In the duskward-directed magnetic field, the polarization pattern was in accordance with vortices as illustrated in Figure 3(b). The magnetic field variation was rather linearly polarized except for the high frequency component near the wake boundary at around 19:13 and 19:52. Again no clear velocity shear was found in the wake boundary (not shown here).

3.3 Off-midnight meridian orbit

In the previous sections we have seen observations along nearly noon-midnight meridians. In such an orbit Kaguya traverses wake boundary in a short time under the condition of B_y-dominated magnetic field. To investigate spatial variations in a longer time, we have chosen an orbit near the wake boundary just behind the duskside terminator. Figure 8 shows the orbit and the spectra of the magnetic field variation obtained by Kaguya on 29 May, 2008. The upstream solar wind ion number density was about 3.3×10^6 m^{-3} and ion bulk speed was 470 km/s according to ACE observation. The background magnetic field was B_y-dominated with smaller B_x component. Kaguya was ascending along an orbit toward the north pole (Figure 8 (c)) in duskward-directed magnetic field (Figure 8 (k)). A yellow curve in Figure 8 (j) represents spacecraft distance $\sqrt{Y_{sse}^2+Z_{sse}^2}$ from the X_{sse} axis. Shallow concave of the yellow curve indicates that the spacecraft did not enter the deep wake.

Figure 8 (g) shows that Kaguya observed right-hand polarized magnetic variation in the southern hemisphere and left-hand polarized rotation in the northern hemisphere, consistently with Figure 3 (b). Figure 8 (h) shows that the polarization was again almost linear except for high frequency parts. The dominant variation was in X_{sse} direction as recognized in Figure 8 (k). The direction of the **k** vector was nearly parallel to the background magnetic field (Figure 8 (i)).

Figure 9 shows the ion velocity for the same period. Shallow entry into the wake enabled IMA observation in the wake. The ion density decreased gradually down to 0.03 $\times10^6$ m^{-3}. The ion bulk speed was nearly constant. Around the crossing of southern wake boundary at 20:41, the x component V_x of ions became slower than those outside the wake and in unperturbed solar wind observed by ACE (green dots), while no such variation was found at the northern wake boundary (21:00-21:15). On the other hand, there was no difference in wave activity between the two crossings of the wake boundary in Figure 8. The spatial variation in V_x is not likely to be essential for the wave activity in the wake.

Figure 8 also shows that the presence of small B_x component did not affect the polarization reversal. The situation was the same for the cases in which B_x and B_y were comparable, as in the nominal solar wind magnetic field parallel to the Archimedean spiral direction. This type of polarization structure was almost always observed only if the magnetic field was stable.

It should also be noted in Figure 8(g) that the right-handed, unified polarization started at 20:32 before Kaguya entered the umbra of the moon at 20:41. Figure 8 (d) shows the position of Kaguya viewed from the Sun. The spacecraft was on the downstream side of the terminator but exposed to the solar wind at 20:32 when the right-handed polarization started. Decrease of ion number density also began nearly the same time. It may due to an intense magnetic anomaly in the southern polar region. On the other hand, there is no such intense crustal field in the northern polar region, but the left-handed polarization persisted until 21:19, when Kaguya was well out of the wake boundary. It might suggest that the unified polarization was formed in the solar wind outside the wake, not in the wake boundary.

3.4 Polarization of the wave in the northward magnetic field

Kaguya's passage through the lunar wake was restricted in north-south direction because of its polar orbit. It's not possible to examine dawn-dusk asymmetry within a single passage through the wake. Instead, an attempt was made to examine cases in northward magnetic field in which Kaguya moved along the background magnetic field in the wake.

Figure 10 shows dynamic spectra of the magnetic field variation observed on 27 February 2009 in the dawnside hemisphere of the lunar wake under the condition of B_z -dominated magnetic field. The upstream solar wind density observed by ACE was 4.3×10^6 m^{-3} and the velocity was 574 km/s during the period corresponding to the Kaguya passage through the wake. Kaguya entered the wake from the southern side at 2:05, crossed the equator at 2:29 and got out of the wake on the northern side at 2:53. Polarization of the magnetic field variation was predominantly left-handed until 2:47, consistently with the pattern as illustrated in Figure 3(b) in the northward-directed magnetic field. After 2:47, the B_y -component of the background magnetic field became large and the polarization turned to be right-handed according to the situation of Figure 3 (a) in the dawnward magnetic field. No north-south asymmetry was found in the polarization of the magnetic field variation. The magnetic field vectors rotated in the same direction throughout the wake over the dawnside hemisphere as far as the direction of the background magnetic field remained the same.

4 Discussion

We have seen that the low frequency magnetic field variation in the lunar wake were left-hand polarized in the southern hemisphere and right-hand polarized in the northern hemisphere in a dawnward-directed magnetic field, and the polarization reversed in a duskward-directed magnetic field as illustrated in Figure 3. In a northward-directed magnetic field, the polarization was left-handed in the dawnside hemisphere and right-handed in the duskside hemisphere, again consistently with Figure 3.

The sense of rotation of the magnetic field variation looks like that of a surface wave generated by Kelvin-Helmholtz (K-H) instability, but it does not account for the observation. The energy source of K-H instability is a velocity shear at a boundary, but the waves in this paper were not always accompanied by such velocity shear. In some cases, a depression of x component of ion bulk velocity V_x was detected in the wake boundary, but it often occurred

that no such decrease was detected in the boundary of the other side of the wake. In addition, the waves were not confined within the wake boundary but found in the center of the wake. It is concluded that the magnetic field variations observed were not surface waves generated by K-H instability.

A velocity shear is not expected at the wake boundary. Differently from those at the Earth's magnetopause, the magnetic field lines in the lunar wake are open to interplanetary space. The solar wind ions can fill in the wake along the magnetic field. Results from 2-dimensional electromagnetic particle-in cell simulations by Nakagawa (2013) and Nakagawa and Kimura (2011) show that ion deceleration in X_{sse} direction may present due to the pressure gradient, but it is much smaller than acceleration in Y_{sse} direction toward the center of the wake. A 3-dimensional hybrid simulation by Holmström et al. (2012) also gave the same result.

The power density of the magnetic field variation was smaller in the center of the wake than in the wake boundary and it eh solar wind outside, suggesting that the waves were generated at the boundary or outside of the wake. There is no signature of wave generation in the wake boundary. In Figure 7 we have seen the unified polarization downstream of the terminator but outside of the wake boundary. It is expected that some interaction between the solar wind and the moon causes the unified polarization, but the mechanism is not yet understood.

The wave mode is thought to be shear Alfvén wave because the magnetic field variation was perpendicular to the background magnetic field. Figure 11 shows the angle between the maximum variance direction and the background magnetic field for the 4 events we have examined. The angle was close to 90° in the wake of all the cases as well as in the solar wind. The maximum variance direction can be obtained more precisely when the waves were nearly linearly polarized. On the other hand, the minimum variance direction becomes less accurate, and this is why the direction of **k** vector varied from event to event. Figure 8 (i) shows **k** vectors nearly parallel to the background magnetic field, while those in Figure 10 (i) were rather perpendicular to the field.

The shear Alfvén wave can propagate into the deepest wake along a field line. In the lunar wake, ion number density drops off by about two orders while magnitude of the magnetic field remains the same, and the Alfvén velocity can be about 10 times higher in the center of the wake than outside, for example, about 500 km/s in the wake. The travel time across the diameter of the wake may be smaller than the gyro period of protos. On the other hand, Figure 4 shows that the magnitude as well as the components of the magnetic field was variable, indicating that the waves were compressional. There might be a coupling of shear Alfvén mode and compressional mode.

The polarization was almost linear for all the events. The linear polarization is consistent with magnetohydrodynamc theory in the limit of frequency ω negligibly small compared with the proton cyclotron frequency Ω_i, but for these events, the frequency was not lower than $0.1\,\Omega_i$. The reason of linear polarization at this frequency range is not yet understood. High frequency components of about 3 times of proton cyclotron frequency were circularly polarized and propagating nearly parallel to the background magnetic field. Generation of these higher frequency waves are also not known. It should be noted that left-hand polarized waves as well as right-handed waves were detected at frequency higher than the proton cyclotron frequency, which are prohibited in dispersion relation. The propagation direction is not likely to cause Doppler shift and no explanation is yet found.

5 Conclusions

Unified polarization of the magnetic field variation was observed by Kaguya in the lunar wake in a frequency range from 0.01 to 0.3 Hz. The polarization reversed at equator crossings under the condition of background magnetic field in dawn-dusk direction. The polarization was highly elliptic and almost linear, except for high frequency component with circular polarization. The waves were shear Alfven mode with compressional component. The wave penetrated into the very center of the wake, suggesting that they were not propagating along a surface of wake boundary. The waves were not always accompanied by velocity shear at the wake, indicating that they were not generated by Kelvin-Helmholtz instability.

Acknowledgments

The authors thank the Kaguya MAP-LMAG and MAP-PACE teams for the Kaguya magnetic field and plasma particle data. The authors also thank the ACE SWEPAM instrument team and the ACE Science Center for providing the ACE data. T.N. thanks Yukai Sawasato and Yusuke Shiga for their contribution in event finding, examination of ion velocity in the lunar wake, and assessment of solar wind condition. The Kaguya MAP-LMAG and MAP-PACE data are available at Kaguya (SELENE) Data Archive (http://l2db.selene.darts.isas.jaxa.jp/index.html.en). The ACE SWEPAM and MAG data are available at http://www.srl.caltech.edu/ACE/ASC/level2/. The authors declare that they have no conflicts of interests. This work was supported by JSPS KAKENHI Grant Number 18K03727.

References

Bale, S.D., Owen, C. J., Bougeret, J.-L., Goetz, K., Kellogg, P. J., Lepping, R. P., Manning, R., & Monson, S. J. (1997), Evidence of currents and unstable particle distributions in an extended region around the lunar plasma wake, Geophys. Res. Lett., 24, 1427-1430, doi:10.1029/97GL01193.

Bosqued, J. M., Lormant, N., Rème, H., d'Uston, C., Lin, R. P., Anderson, K. A., Carlson, C. W., Ergun, R. E., Larson, D., McFadden, J., McCarthy, M. P., Parks, G. K., Sanderson, T. R., & Wenzel, K.-P. (1996), Moon-solar wind interaction: First results from the WIND/3DP experiment, Geophys. Res. Lett., 23, 1259-1262, doi:10.1029/96GL00303.

Colburn, D. S., Currie, R. G., Mihalov, J. D., & Sonett, C. P. (1967), Diamagnetic solar-wind cavity discovered behind moon, Science 158, 3804, pp. 1040-1042, doi: 10.1126/science.158.3804.1040.

Farrell, W. M., Fitzenreiter, R. J., Owen, C. J., Byrnes, J. B., Lepping, R. P., Ogilvie, K. W., &Neubauer, F. (1996), Upstream ULF waves and energetic electrons associated with the lunar wake: Detection of precursor activity, Geophys. Res. Lett., 1271–1274, doi:10.1029/96GL01355.

Fowler, R. A., Kotick, B. J., & Elliott, R. D. (1967), Polarization analysis of natural and artificially induced geomagnetic micropulsations, J. Geophys. Res., 72(11), 2871–2883, doi:10.1029/JZ072i011p02871.

Halekas, J. S., Brain, D. A., Mitchell, D. L., & Lin, R. P. (2006). Whistler waves observed near lunar crustal magnetic sources. Geophysical Research Letters, 33, L22104. https://doi.org/10.1029/2006GL027684.

Harada, Y., Halekas, J. S., Poppe, A. R., Tsugawa, Y., Kurita, S., & McFadden, J. P. (2015), Statistical characterization of the foremoon particle and wave morphology: ARTEMIS observations. J. Geophys. Res. Space Physics, 120, 4907– 4921. doi: 10.1002/2015JA021211.

Harada, Y., & Halekas, J. S. (2016), Upstream Waves and Particles at the Moon, in *Low-Frequency Waves in Space*, chap. 18, pp. 307–322, John Wiley Sons, Inc, Hoboken, NJ, doi: 10.1002/9781119055006.

Holmström, M., Fatemi, S., Futaana, Y. & H. Nilsson (2012), The interaction between the Moon and the solar wind, Earth Planet. Space 64, 237–245, https://doi.org/10.5047/eps.2011.06.040.

Kato, M., Sasaki, S., Takizawa, Y. & the Kaguya project team (2010), The Kaguya mission overview, *Space Sci. Rev.*, 154, 3–19, doi:10.1007/s11214-010-9678-3.

Krall, N. A., & Tidman, D. A. (1969), Magnetic field fluctuations near the Moon, J. Geophys. Res., 74(26), 6439– 6443, doi:10.1029/JA074i026p06439.

Lyon, E. F., Bridge, H. S., & Binsack, J. H. (1967), Explorer 35 plasma measurements in the vicinity of the Moon, J. Geophys. Res., 72(23), 6113– 6117, doi:10.1029/JZ072i023p06113.

Lue, C., Futaana, Y., Barabash, S., Wieser, M., Holmström, M., Bhardwaj, A., Dhanya, M. B., & Wurz, P. (2011), Strong influence of lunar crustal fields on the solar wind flow, Geophys. Res. Lett., 38, L03202, doi:10.1029/2010GL046215.

McComas, D. J., Allegrini, F., Bochsler, P., Frisch, P., Funsten, H. O., Gruntman, M., Janzen, P. H., Kucharek, H., Möbius, E., Reisenfeld, D. B., & Schwadron, N. A. (2009), Lunar backscatter and neutralization of the solar wind: First observations of neutral atoms from the Moon, Geophys. Res. Lett., 36, DOI: 10.1029/2009GL038794.

Nakagawa, T. (2013), Ion entry into the wake behind a nonmagnetized obstacle in the solar wind: Two-dimensional particle-in-cell simulations, J. Geophys. Res., 118, 1849-1860, doi:10.1002/jgra.50129.

Nakagawa, T. (2016), ULF/ELF waves in the near-Moon space, in *Low-Frequency Waves in Space*, chap. 17, pp. 295–306, John Wiley Sons, Inc, Hoboken, NJ, doi:10.1002/9781119055006.

Nakagawa, T., and S. Kimura (2011), Role of the solar wind magnetic field in the interaction of a non-magnetized body with the solar wind: An electromagnetic 2-D particle-in-cell simulation, Earth Planets Space, 63(6), 477-486, doi:10.5047/eps.2011.02.006.

Nakagawa, T., Takahashi, F., Tsunakawa, H., Shibuya, H., Shimizu, H., & Matsushima, M. (2011), Non-monochromatic whistler waves detected by Kaguya on the dayside surface of the moon. Earth, Planet. Space, 63, 37–46, doi:10.5047/eps.2010.01.005

Nakagawa, T., Nakayama, A., Takahashi, F., Tsunakawa, H., Shibuya, H., Shimizu, H., & Matsushima, M. (2012), Large-amplitude monochromatic ULF waves detected by Kaguya at the moon. Journal of Geophysical Research, 117, A04101, doi:10.1029/2011JA017249.

Nakagawa, T., Nakashima, T., Wada, T., Tsunakawa, H., Takahashi, F., Tsunakawa, H., Shibuya, H., Shimizu, H., & Matsushima, M. (2015), ELF magnetic fluctuations detected by Kaguya in deepest lunar wake associated with type-II protons, Earth Planet Space 67, 50, doi:10.1186/s40623-015-0196-0.

Ness, N. F., Behannon, K. W., Taylor, H. E., & Whang, Y. C. (1968), Perturbations of the interplanetary magnetic field by the lunar wake, J. Geophys. Res., 73(11), 3421–3440, doi:10.1029/JA073i011p03421.

Ness, N. F., & Schatten, K. H. (1969), Detection of interplanetary magnetic field fluctuations stimulated by the lunar wake, J. Geophys. Res., 74(26), 6425– 6438, doi:10.1029/JA074i026p06425.

Nishino, M. N., Fujimoto, M., Maezawa, K., Saito, Y., Yokota, S., Asamura, K., Tanaka, T., Tsunakawa, H., Matsushima, M., Takahashi, F., Terasawa, T., Shibuya, H., & Shimizu, H. (2009), Solar-wind proton access deep into the near-Moon wake, Geophys. Res. Lett., 36, L16103, doi:10.1029/2009GL039444.

Nishino, M. N., Fujimoto, M., Saito, Y., Yokota, S., Kasahara, Y. Omura, Y., Goto, K., Hashimoto, K., Kumamoto, A., Ono, T., Tsunakawa, H., Matsushima, M., Takahashi, F., Shibuya, H. Shimizu, H., & Terasawa, T. (2010), Effect of the solar wind proton entry into the deepest lunar wake, Geophys. Res. Lett., 37, 12106, doi:10.1029/2010GL043948.

Nishino, M., Saito, Y., Tsunakawa, H., Kasahara, Y., Kawamura, M., Matsushima, M., Takahashi, F., Shibuya, H., Shimizu, H., Goto, Y., Hashimoto, K., Omura, Y., Kumamoto, A., Ono, T., & Yokota, S. (2013), Type-II entry of solar wind protons into the lunar wake: Effects of magnetic connection to the night-side surface, Planet. Space Sci., 87, 106-114, doi:10.1016/j.pss.2013.08.017.

Ogilvie, K. W., Steinberg, J. T., Fitzenreiter, R. J., Owen, C. J., Lazarus, A. J., Farrell, W. M., Torbert, R. B. (1996), Observation of the lunar plasma wake from the WIND spacecraft on December 27, 1994, Geophys. Res. Lett., 23, 1255-1258, doi:10.1029/96GL01069.

Poppe, A. R., Sarantos, M., Halekas, J. S., Delory, G. T., Saito, Y. Nishino, M. (2014), Anisotropic solar wind sputtering of the lunar surface induced by crustal magnetic anomalies, Geophys. Res. Lett., 41, 4865–4872, doi:10.1002/2014GL060523.

Saito, Y., S. Yokota, T. Tanaka, K. Asamura, M. N. Nishino, M. Fujimoto, H. Tsunakawa, H. Shibuya, M. Matsushima, H. Shimizu, F. Takahashi, T. Mukai, T. Terasawa (2008), Solar wind proton reflection at the lunar surface: Low energy ion measurement by MAP-PACE onboard SELENE (Kaguya), Geophys. Res. Lett., 35, L24205, doi:10.1029/2008GL036077.

Saito, Y., Yokota, S., Asamura, K., Tanaka,T., Nishino, M. N., Yamamoto, T., Terakawa, Y., Fujimoto, M., Hasegawa, H., Hayakawa, H., Hirahara, M., Hoshino, M., Machida, S., Mukai, T., Nagai, T., Nagatsuma, T., Nakagawa, T., Nakamura, M., Oyama, K.-I., Sagawa, E., Sasaki, S., Seki, K., Shinohara, I., Terasawa, T., Tsunakawa, H., Shibuya, H., Matsushima, M., Shimizu, H., & Takahashi, F. (2010), In-flight performance and initial results of Plasma energy Angle and Composition Experiment (PACE) on SELENE (Kaguya), Space Sci. Rev., 154, 265-303, doi:10.1007/s11214-010-9647-x.

Saito, Y., Nishino, M. N., Fujimoto, M., Yamamoto, T., Yokota, S., Tsunakawa, H., Shibuya, H., Matsushima, M., Shimizu, H. & Takahashi, F. (2012), Simultaneous observation of the electron acceleration and ion deceleration over lunar magnetic anomalies, Earth Planet. Space, 64(2), 83-92, doi:10.5047/eps.2011.07.011.

Schubert, G. & Lichtenstein, B. R. (1974), Observations of moon-plasma interactions by orbital and surface experiments, Rev. Geophys. Space Phys., 12, 592-626.

Shimizu, H., Takahashi, F., Horii, N., Matsuoka, A., Matsushima, M., Shibuya, H., & Tsunakawa, H. (2008), Ground calibration of the high-sensitivity SELENE lunar magnetometer LMAG. Earth, Planets and Space, 60, 353–363, doi:10.1186/BF03352800.

Sonnerup, B. U. Ö. & Cahill, L. J. (1967), Magnetopause structure and attitude from Explorer 12 observations, J. Geophys. Res., 72(1), 171– 183, doi:10.1029/JZ072i001p00171.

Takahashi, F., Shimizu, H., Matsushima, M., Shibuya, H., Matsuoka, A., Nakazawa, S., Iijima, Y., Otake, H., & Tsunakawa, H. (2009). In-orbit calibration of the lunar magnetometer onboard SELENE (KAGUYA). Earth, Planets and Space, 61, 1269–1274, doi:10.1186/BF03352979.

Tsugawa, Y., Terada, N., Katoh, Ono, T., Tsunakawa, H., Takahashi, F., Shibuya, H., Shimizu, H., & Matsushima, M. (2011), Statistical analysis of monochromatic whistler waves near the Moon detected by Kaguya, Ann. Geophys., 29, 889–893, doi:10.5194/angeo-29-889-2011.

Tsugawa, Y., Katoh, Y., Terada, N., Y., Ono, T., Tsunakawa, H., Takahashi, F., Shibuya, H., Shimizu, H., Matsushima, M., Saito, Y., Yokota, S., & Nishino, M. N. (2012), Statistical study of broadband whistler-mode waves detected by Kaguya near the Moon, Geophys. Res. Lett., 39, L16101, doi:10.1029/2012GL052818.

Tsunakawa, H., Shibuya, H., Takahashi, F., Shimizu, H., Matsushima, M., Matsuoka, A., Nakazawa, S., Otake H., & Iijima Y. (2010), Lunar magnetic field observation and initial global mapping of lunar magnetic anomalies by MAP-LMAG onboard SELENE (Kaguya), Space Sci. Rev., 154, 219-251, doi:10.1007/s11214-010-9652-0.

Wieser, M., Barabash, S., Futaana, Y., Holmström, M., Bhardwaj, A., Sridharan, R., Dhanya, M.B., Wurz, P., Schaufelberger, A., Asamura, K. (2009), Extremely high reflection of solar wind protons as neutral hydrogen atoms from regolith in space, Planet. Space Sci., 57, 2132-2134, doi:10.1016/j.pss.2009.09.012

Wieser, M., Barabash, S., Futaana, Y., Holmström, M., Bhardwaj, A., Sridharan, R., Dhanya, M.B., Wurz, P., Schaufelberger, A., Asamura, K. (2011), Erratum to “Extremely high reflection of solar wind protons as neutral hydrogen atoms from regolith in space”, Planet. Space Sci., 57, 798-799, doi:10.1016/j.pss.2011.01.016.

Figure 1. An example of polarization reversal observed by Kaguya on 30 March 2008. The sense of rotation of magnetic field variation switched from left-hand in the southern hemisphere to right-hand in the northern hemisphere. (a) The position of the moon in the Geocentric Solar Ecliptic (GSE) coordinates, with the nominal bow shock (BS) and magnetopause (MP). (b–d) The trajectory of Kaguya encircling the moon, projected onto the (b) x-y and (c) x-z plane of Selenocentric Solar Ecliptic (SSE) coordinates, and (d) y-z plane of the Mean Earth/Polar Axis (ME) coordinates. Thin-lined curves show that the spacecraft was behind the moon. (e) Number densities of ions measured by IEA (pink), IMA (orange), combination of both (red) and of electrons (gray). (f) The dynamic spectrum of the power density obtained by 120-s Fourier transform of the 1s averages of the magnetic field. (g) Polarization of each frequency component of the magnetic field variation with energy density higher than 0.1 nT^2/Hz. The left (right)-handed polarization with respect to the background magnetic field is colored with blue (red). (h) The ellipticity of the magnetic field variation defined as the ratio of the length of the semi-minor (intermediate variance) axis to the length of the semi-major (maximum variance) axis of the polarization ellipse of each Fourier component. (i) The angle between the k vector and the background magnetic field. (j) The Kaguya position and (k) the 1s averages of the magnetic field in the SSE coordinates. The yellow curve in panel (j) is the spacecraft distance $\sqrt{Y_{sse}^2 + Z_{sse}^2}$ from the X_{sse} axis. Vertical dashed lines indicate the spacecraft crossings of the nominal wake boundaries ($\sqrt{Y_{sse}^2 + Z_{sse}^2}$ = 1 R_L).

Figure 2. Coherence of the magnetic variations observed by Kaguya during the same period in Figure 1 on 30 March 2008. Fourier components whose power density was greater than 01 nT^2/Hz were displayed. From top to bottom, coherence between the magnetic field components (a) B_x and B_y, (b) B_y and B_z, and (c) B_z and B_x. Bottom panel shows the position of Kaguya in SSE coordinates.

Figure 3. Schematic illustrations of the direction of rotation of the magnetic field variation in the lunar wake. Red (blue) arrays indicate the right-handed (left-handed) polarization with respect to the background magnetic field, respectively. Black arrays represent solar wind flow outside the wake.

Figure 4. Examples of spectra and waveforms observed by Kaguya in the wake. (a) 7:04-7:06, (b) 7:06–7:08, (c) 7:19–7:21, (d) 7:38–7:40 and (e) 7:42-7:43 on 30 March 2008. Gray, green, red and black curves in the left panels show spectra of magnetic field components in minimum, intermediate and maximum directions and of total power, respectively. Differently from those displayed in Figure 1, minimum variance analysis was applied to the time series data of the magnetic field, not the Fourier components. Vertical lines in the left panels indicate local cyclotron frequency of protons. Right panels show waveforms of the magnitude and the components along the direction of maximum, intermediate and minimum variance. Minimum variance analysis was applied to the 2-m period in the middle of each panel, for example, 7:4:0–7:6:0 in panel (a).

534 **Figure 5**. Hodograms of magnetic field vectors observed by Kaguya. Observations for the
535 same periods in Figure 4, (a) 7:04–7:06 and (b) 7:06–7:08 in the southern hemisphere, (c)
536 7:19–7:21 around the equator, (d) 7:38–7:40 and (e) 7:41-7:43 in the northern hemisphere on
537 30 March 2008. Tips of the magnetic field vectors are projected onto the principal axis
538 coordinates with the start points marked with red circles. The minimum variance direction
539 was chosen so that the normal component $\mathbf{B}_0 \cdot \mathbf{n}$ of the background magnetic field should
540 be positive (out from the plane).

541

542 **Figure 6.** Plasma density and bulk velocity in SSE coordinates obtained from MAP-PACE
543 onboard Kaguya in the lunar wale on 30 March 2008. The red curves show the density and
544 bulk velocity of ions for the periods during which both IMA and IEA data were available.
545 The gray curves are electron momenta calculated from combination of the results from ESA-
546 1 and ESA-2.

547

548 **Figure 7**. Another pattern of polarization reversal observed by Kaguya on 7 April 2008.
549 Polarization of magnetic field variation switched from right-hand in the southern hemisphere
550 to left-hand in the northern hemisphere. The format is the same as Figure 1.

551

552 **Figure 8**. Polarization reversal in a shallow entry into the wake observed by Kaguya on 29
553 May 2008. Magnetic field variation turned from right-hand in the southern hemisphere to
554 left-hand in the northern hemisphere. The format is the same as Figure 1 except for panel (d)
555 which shows the orbit of Kaguya in y-z plane of SSE coordinate system, viewed from the
556 sun.

557

558 **Figure 9**. Ion velocity observed by MAP-Pace on 29 May 2008. The format is the same as
559 Figure 6. Green dots are upstream solar wind observation made by ACE at 1.34×10^6 km
560 upstream of the moon and shifted for the travel time.

561

562 **Figure 10**. Polarization reversal in a northward-directed magnetic field, observed by Kaguya
563 on 27 February 2009. Left-hand polarization of magnetic field variation was observed in the
564 dawnside hemisphere in the lunar wake. The format is the same as Figure 1.

565

566 **Figure 11**. The angle between the maximum variance direction and the background magnetic
567 field. Observation by Kaguya around the moon on (a) 30 March, 2008, (b) 7 April, 2008, (c)
568 29 May, 2008, and (d) 27 February, 2009.

Figure 1.

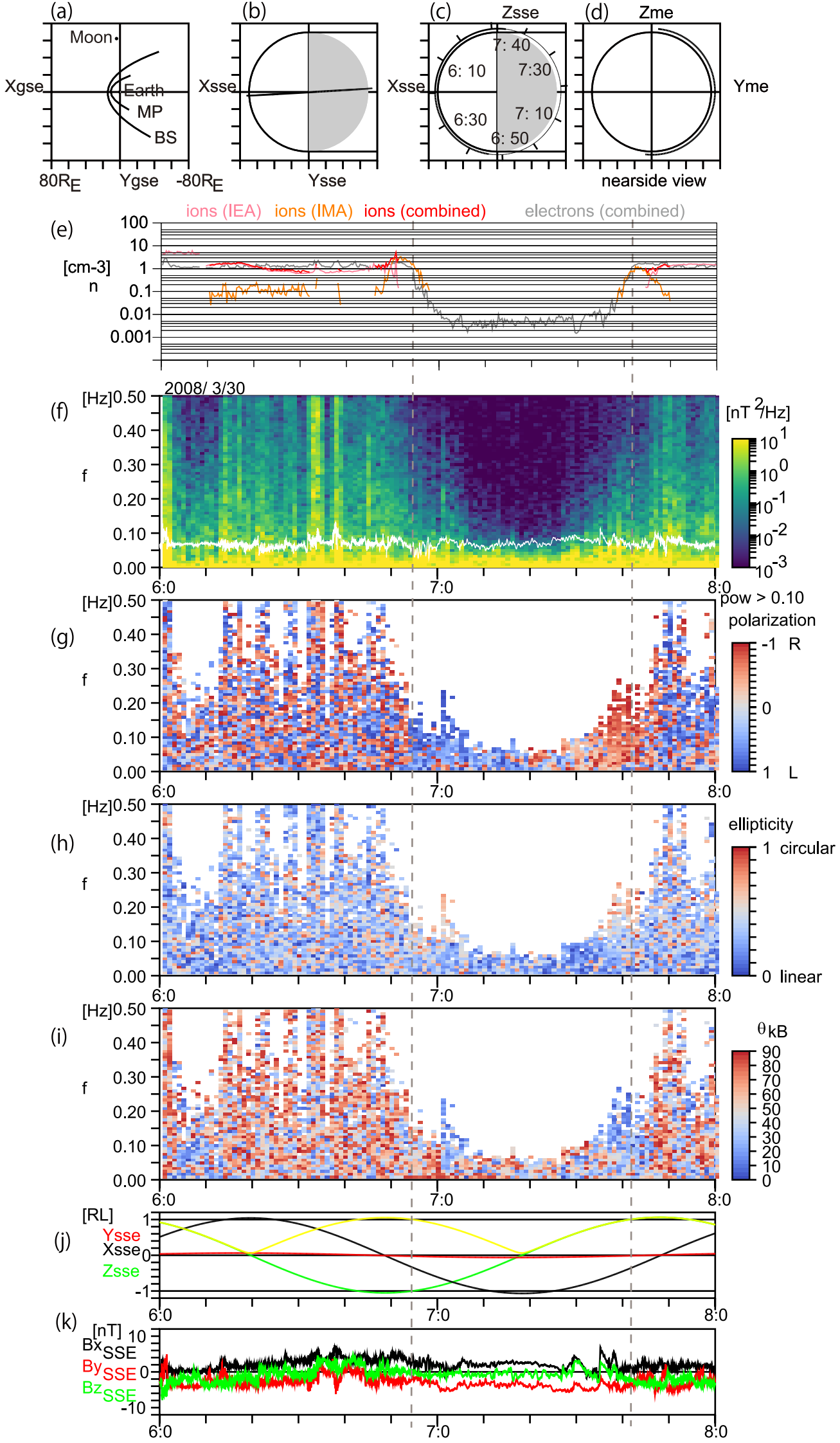
(a)
Moon
Xgse
Earth
MP
BS
80R_E
Ygse
-80R_E
(b)
Xsse
Ysse
(c)
Zsse
Xsse
7: 40
6: 10
7:30
6:30
7: 10
6: 50
(d)
Zme
Yme
nearside view
ions (IEA)
ions (IMA)
ions (combined)
electrons (combined)
(e)
[cm-3]
n
100
10
1
0.1
0.01
0.001
2008/ 3/30
(f)
[Hz]
f
0.50
0.40
0.30
0.20
0.10
0.00
[nT 2/Hz]
10^1
10^0
10^-1
10^-2
10^-3
6:0
7:0
8:0
(g)
pow > 0.10
polarization
-1 R
0
1 L
(h)
ellipticity
1 circular
0 linear
(i)
θkB
90
80
70
60
50
40
30
20
10
0
(j)
[RL]
Ysse
Xsse
Zsse
1
0
-1
(k)
[nT]
Bx SSE
By SSE
Bz SSE
10
0
-10

Figure 2.

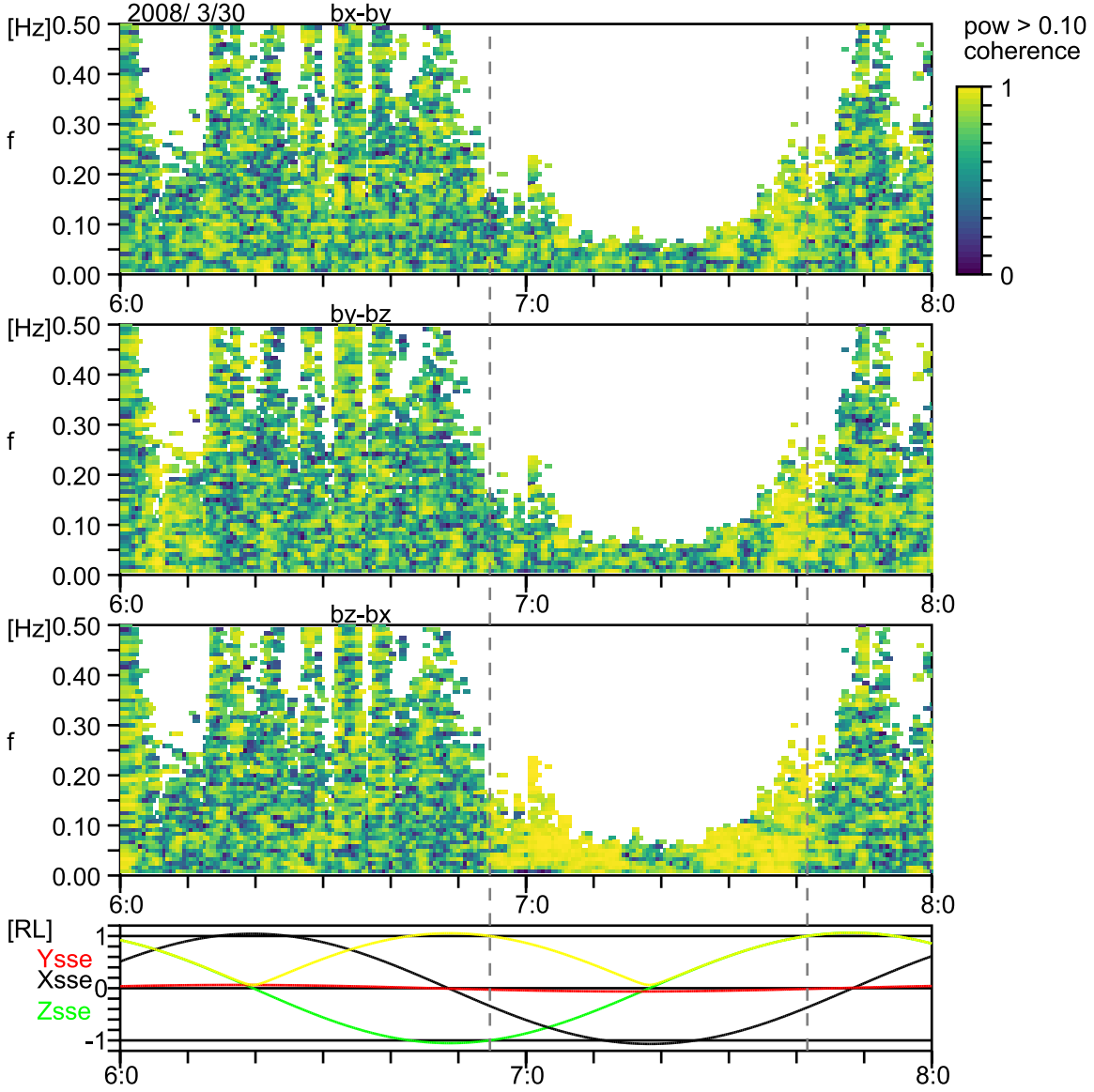
2008/ 3/30
bx-by
by-bz
bz-bx
[Hz]
f
0.50
0.40
0.30
0.20
0.10
0.00
6:0
7:0
8:0
pow > 0.10
coherence
1
0
[RL]
Ysse
Xsse
Zsse
1
0
-1

Figure 3.

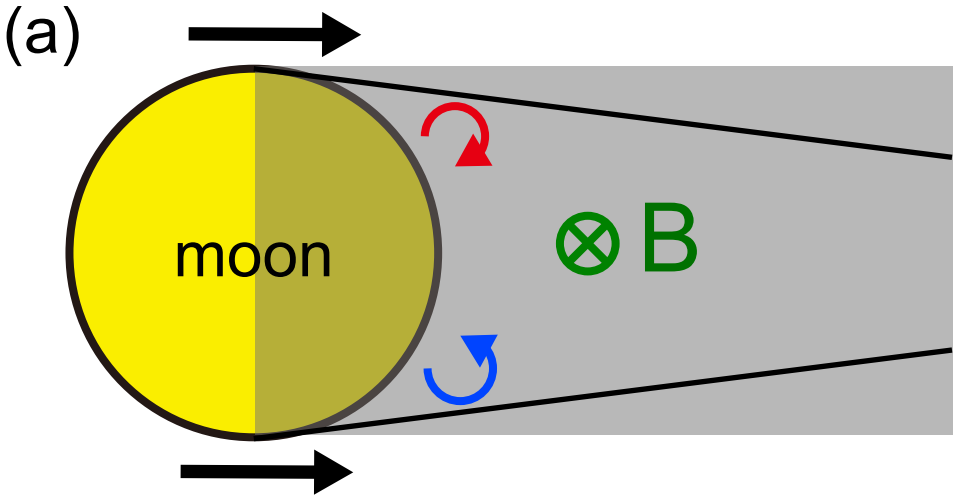
(a)
moon
⊗ B

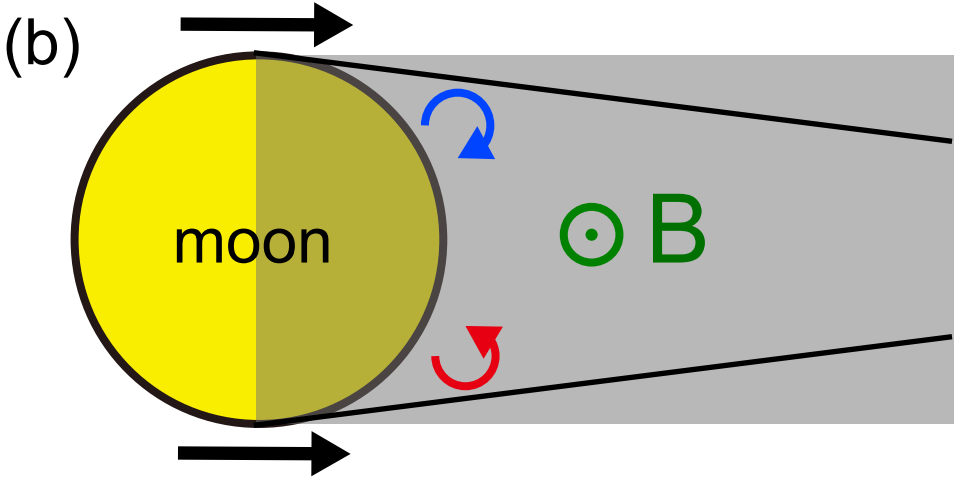
(b)
moon
⊙ B

Figure 4.

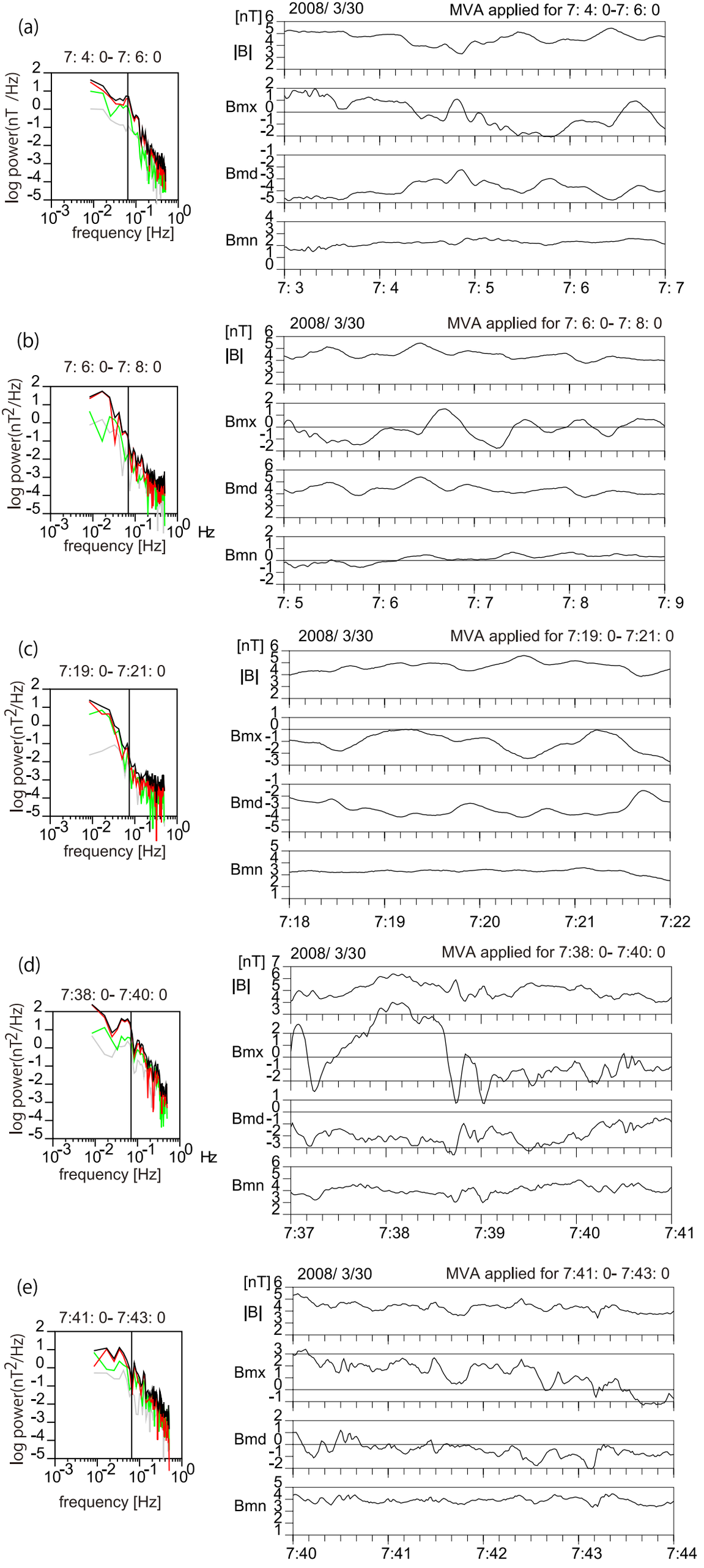
(a)
7: 4: 0- 7: 6: 0
log power(nT /Hz)
frequency [Hz]
2008/ 3/30
MVA applied for 7: 4: 0-7: 6: 0
[nT]
|B|
Bmx
Bmd
Bmn
7: 3
7: 4
7: 5
7: 6
7: 7
(b)
7: 6: 0- 7: 8: 0
log power(nT2/Hz)
Hz
frequency [Hz]
2008/ 3/30
MVA applied for 7: 6: 0- 7: 8: 0
[nT]
|B|
Bmx
Bmd
Bmn
7: 5
7: 6
7: 7
7: 8
7: 9
(c)
7:19: 0- 7:21: 0
log power(nT2/Hz)
frequency [Hz]
2008/ 3/30
MVA applied for 7:19: 0- 7:21: 0
[nT]
|B|
Bmx
Bmd
Bmn
7:18
7:19
7:20
7:21
7:22
(d)
7:38: 0- 7:40: 0
log power(nT2/Hz)
Hz
frequency [Hz]
2008/ 3/30
MVA applied for 7:38: 0- 7:40: 0
[nT]
|B|
Bmx
Bmd
Bmn
7:37
7:38
7:39
7:40
7:41
(e)
7:41: 0- 7:43: 0
log power(nT2/Hz)
frequency [Hz]
2008/ 3/30
MVA applied for 7:41: 0- 7:43: 0
[nT]
|B|
Bmx
Bmd
Bmn
7:40
7:41
7:42
7:43
7:44

Figure 5.

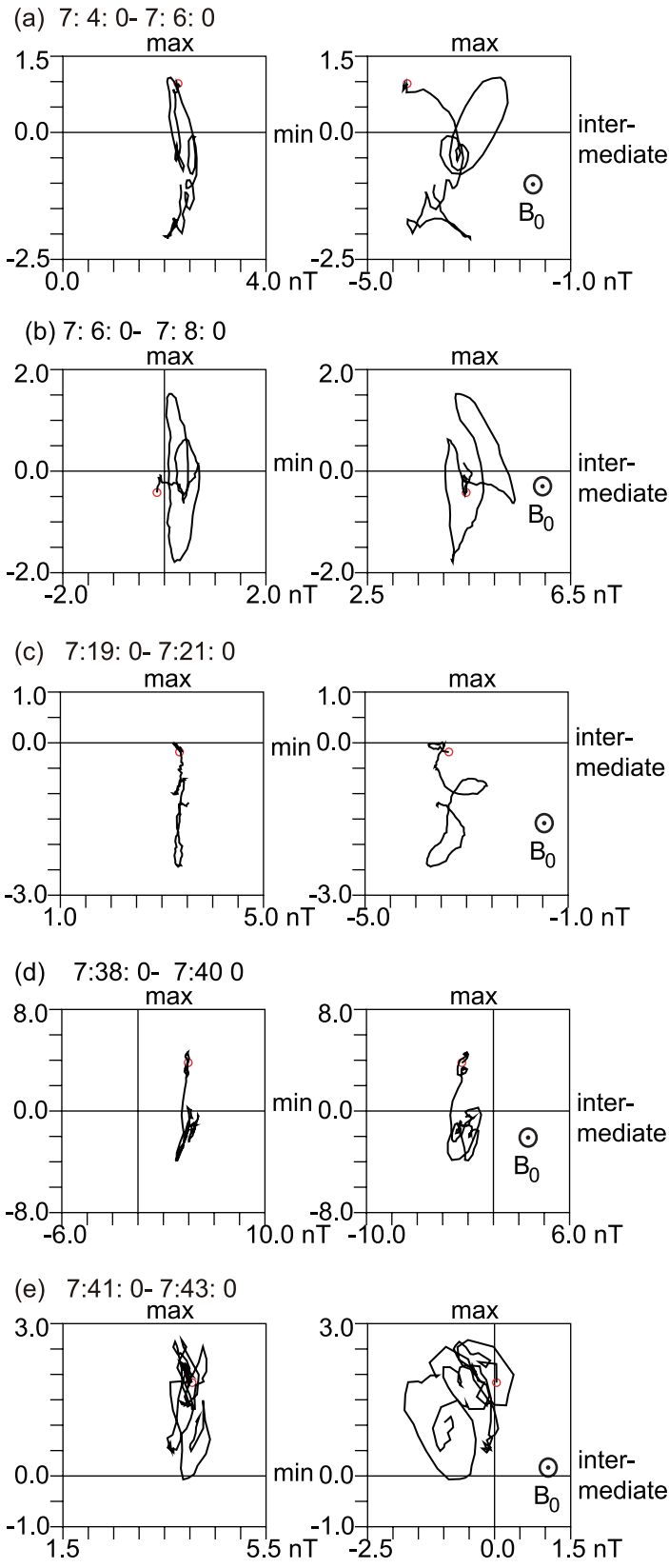
(a) 7: 4: 0- 7: 6: 0
max
1.5
0.0
-2.5
min
0.0
4.0 nT
max
1.5
0.0
-2.5
-5.0
-1.0 nT
inter-
mediate
B0
(b) 7: 6: 0- 7: 8: 0
max
2.0
0.0
-2.0
min
-2.0
2.0 nT
max
2.0
0.0
-2.0
2.5
6.5 nT
inter-
mediate
B0
(c) 7:19: 0- 7:21: 0
max
1.0
0.0
-3.0
min
1.0
5.0 nT
max
1.0
0.0
-3.0
-5.0
-1.0 nT
inter-
mediate
B0
(d) 7:38: 0- 7:40 0
max
8.0
0.0
-8.0
min
-6.0
10.0 nT
max
8.0
0.0
-8.0
-10.0
6.0 nT
inter-
mediate
B0
(e) 7:41: 0- 7:43: 0
max
3.0
0.0
-1.0
min
1.5
5.5 nT
max
3.0
0.0
-1.0
-2.5
0.0
1.5 nT
inter-
mediate
B0

Figure 6.

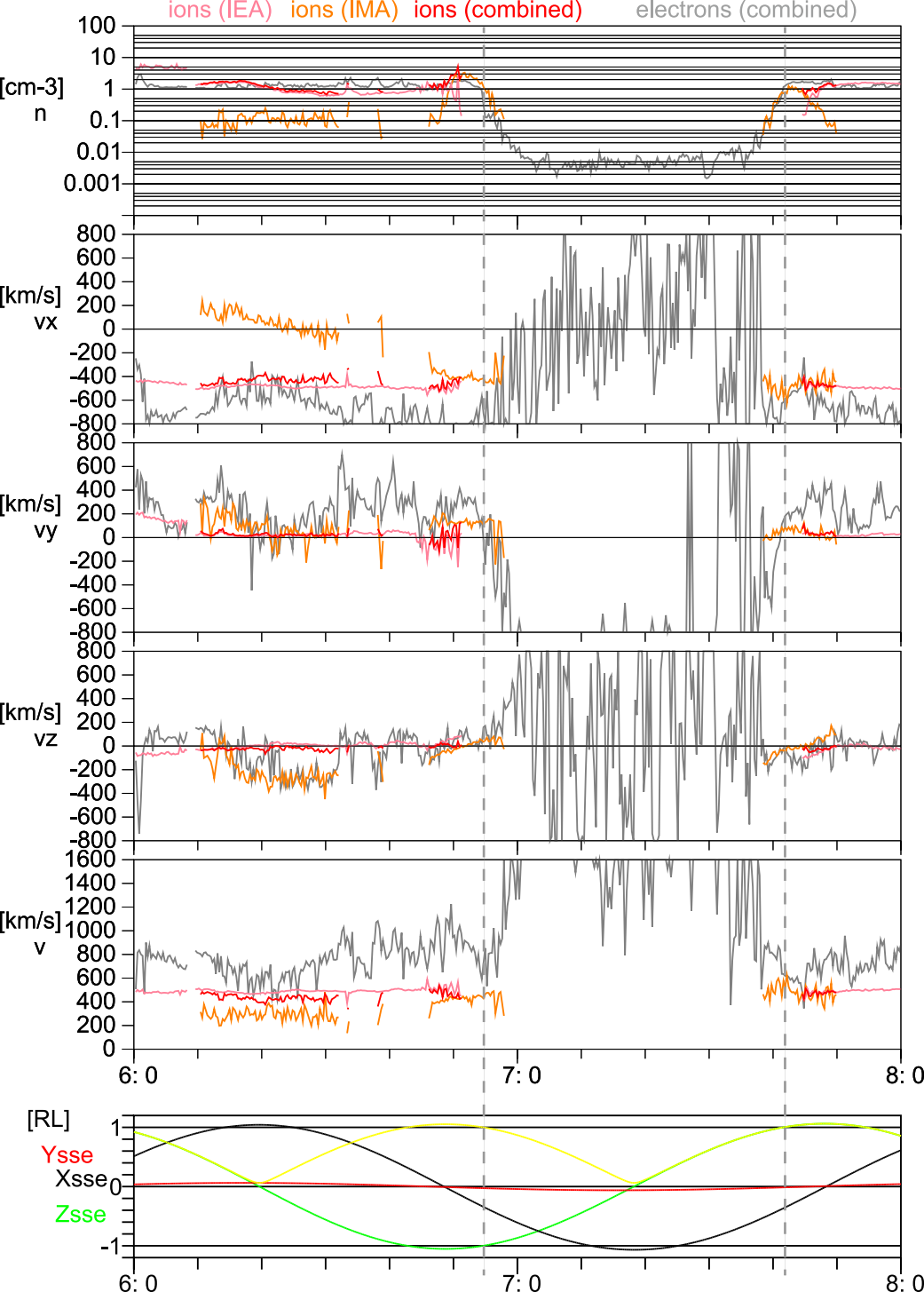
ions (IEA)
ions (IMA)
ions (combined)
electrons (combined)
[cm-3]
n
100
10
1
0.1
0.01
0.001
[km/s]
vx
800
600
400
200
0
-200
-400
-600
-800
[km/s]
vy
[km/s]
vz
[km/s]
v
1600
1400
1200
1000
6: 0
7: 0
8: 0
[RL]
Ysse
Xsse
Zsse
1
0
-1

Figure 7.

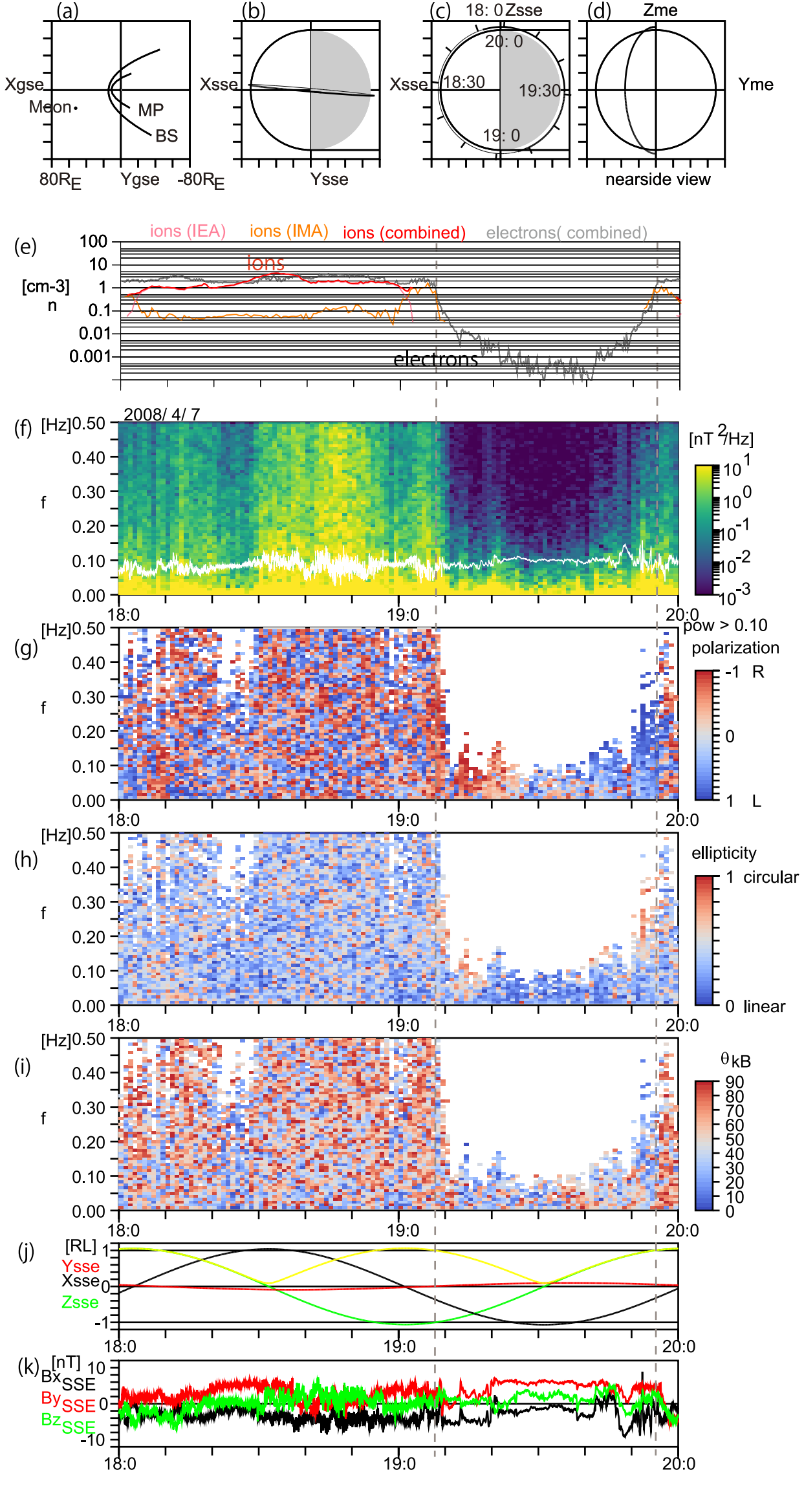
(a)
Xgse
Moon
MP
BS
80R_E
Ygse
-80R_E
(b)
Xsse
Ysse
(c)
18: 0 Zsse
20: 0
Xsse
18:30
19:30
19: 0
(d)
Zme
Yme
nearside view
(e)
ions (IEA)
ions (IMA)
ions (combined)
electrons(combined)
[cm-3]
n
100
10
1
0.1
0.01
0.001
ions
electrons
(f)
2008/ 4/ 7
[Hz]
0.50
0.40
0.30
0.20
0.10
0.00
f
[nT 2/Hz]
10 1
10 0
10 -1
10 -2
10 -3
18:0
19:0
20:0
(g)
pow > 0.10
polarization
-1 R
0
1 L
(h)
ellipticity
1 circular
0 linear
(i)
θkB
90
80
70
60
50
40
30
20
10
0
(j)
[RL]
Ysse
Xsse
Zsse
1
0
-1
(k)
[nT]
Bx SSE
By SSE
Bz SSE
10
0
-10

Figure 8.

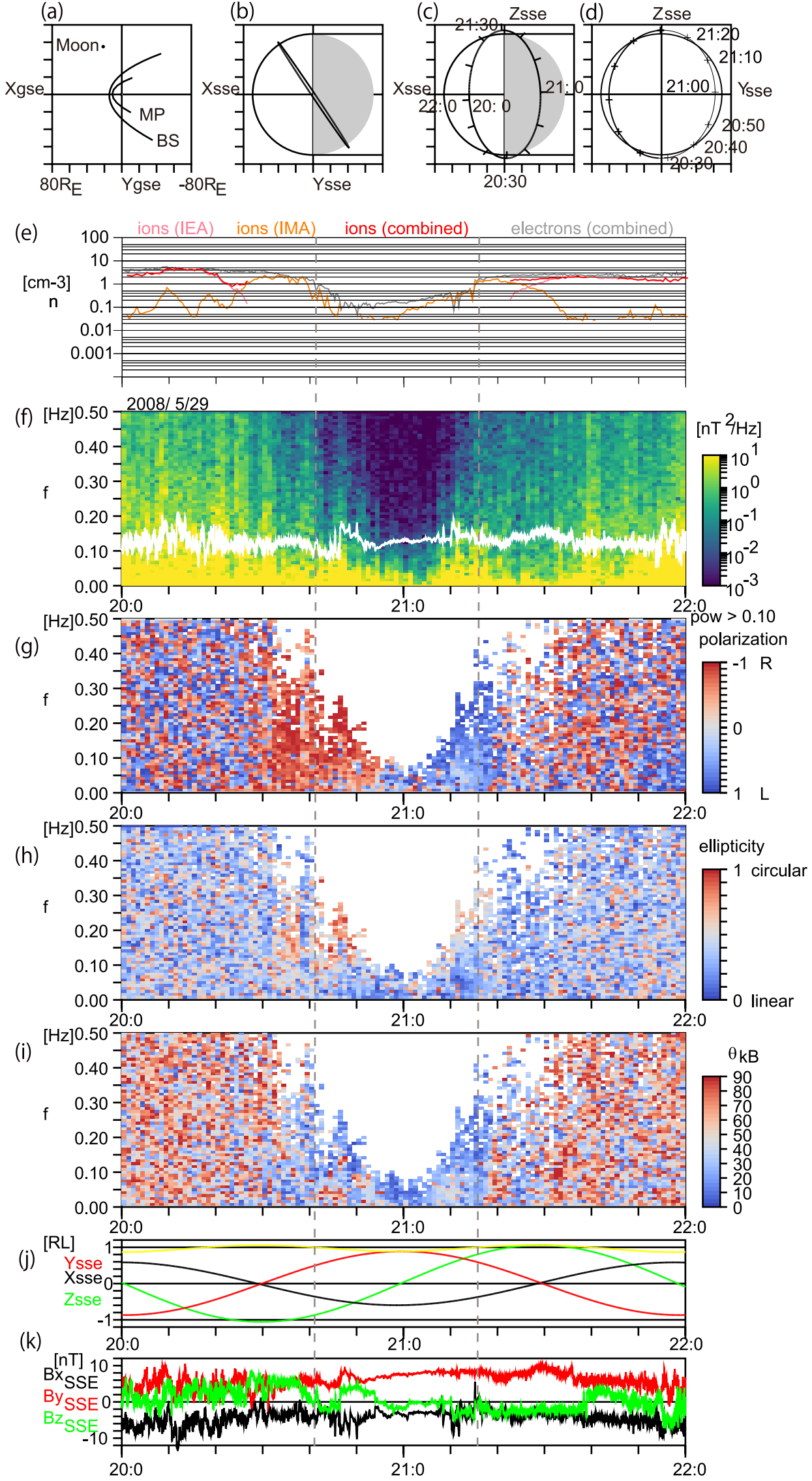
(a)
Moon
Xgse
MP
BS
80RE
Ygse
-80RE
(b)
Xsse
Ysse
(c)
Zsse
21:30
Xsse
22: 0
20: 0
21: 0
20:30
(d)
Zsse
21:20
21:10
21:00
Ysse
20:50
20:40
20:30
(e)
ions (IEA)
ions (IMA)
ions (combined)
electrons (combined)
100
10
[cm-3]
n
1
0.1
0.01
0.001
2008/ 5/29
(f)
[Hz]
0.50
0.40
0.30
f
0.20
0.10
0.00
20:0
21:0
22:0
[nT 2/Hz]
10 1
10 0
10 -1
10 -2
10 -3
(g)
pow > 0.10
polarization
-1 R
0
1 L
(h)
ellipticity
1 circular
0 linear
(i)
θkB
90
80
70
60
50
40
30
20
10
0
(j)
[RL]
Ysse
Xsse
Zsse
1
0
-1
(k)
[nT]
Bx SSE
By SSE
Bz SSE
10
0
-10

Figure 9.

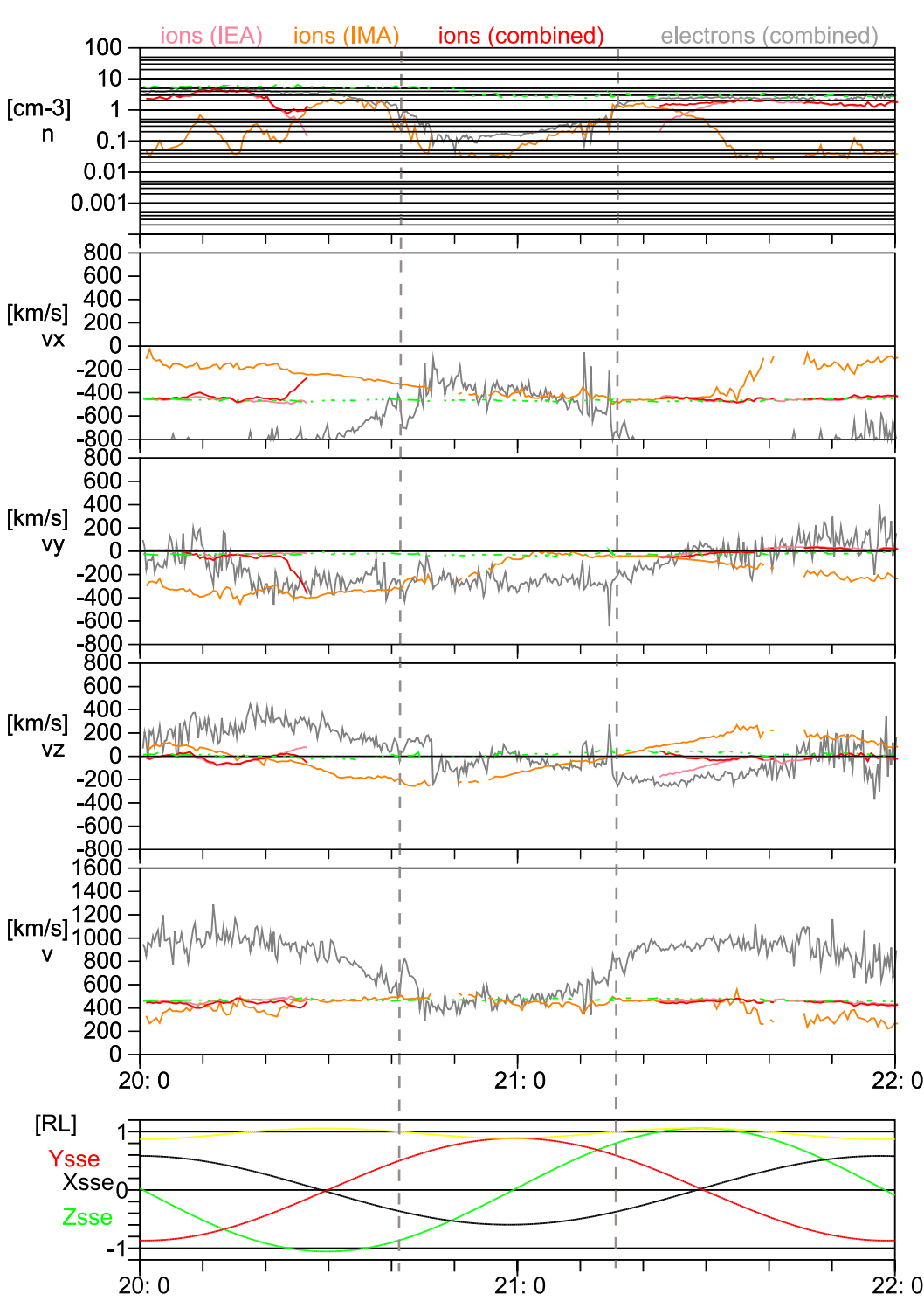
ions (IEA)
ions (IMA)
ions (combined)
electrons (combined)
[cm-3]
n
100
10
1
0.1
0.01
0.001
[km/s]
vx
800
600
400
200
0
-200
-400
-600
-800
[km/s]
vy
[km/s]
vz
[km/s]
v
1600
1400
1200
1000
20: 0
21: 0
22: 0
[RL]
Ysse
Xsse
Zsse
1
0
-1

Figure 10.

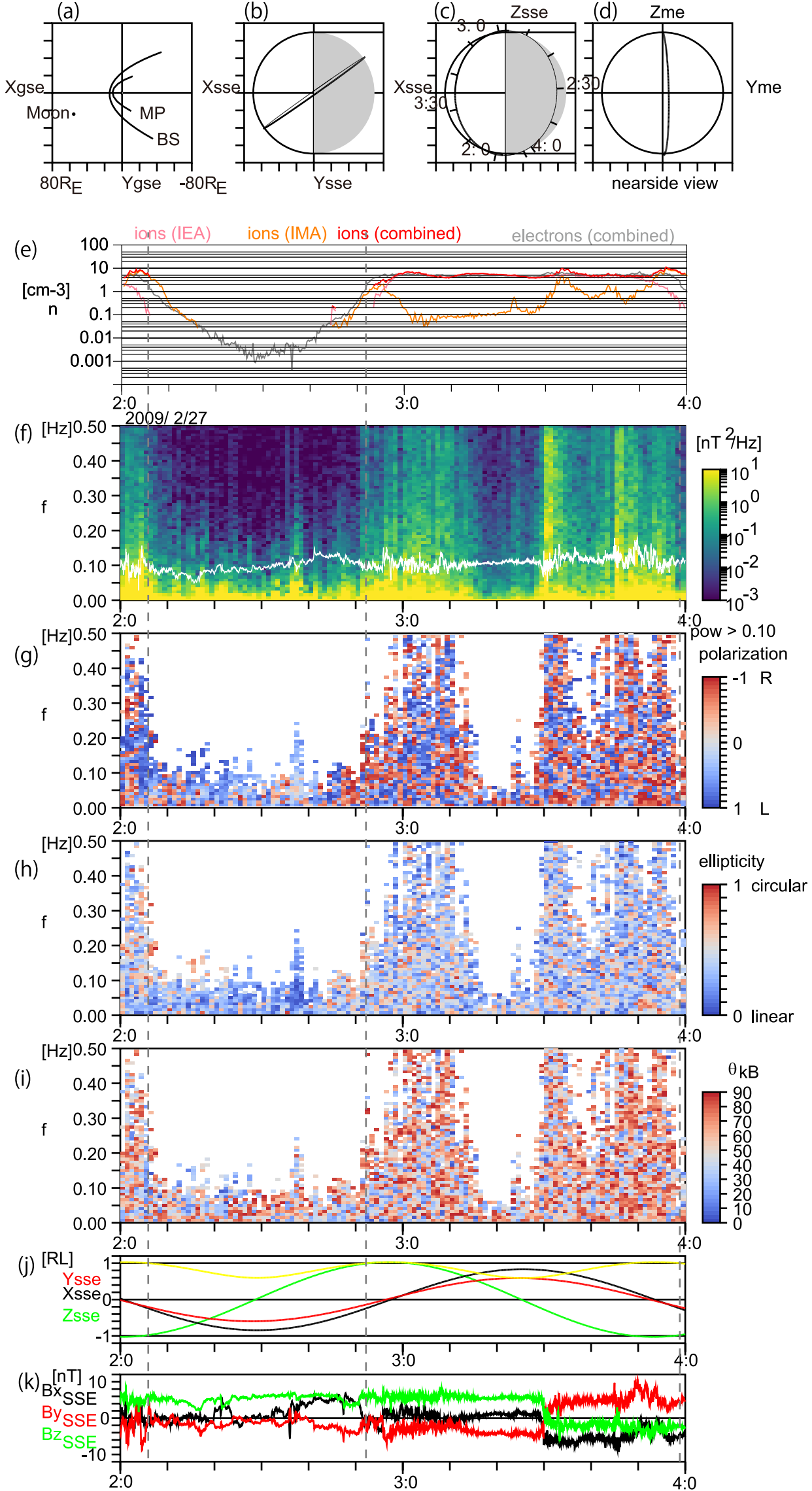
(a)
Xgse
Moon
MP
BS
80RE
Ygse
-80RE
(b)
Xsse
Ysse
(c)
Zsse
Xsse
3:30
2:30
2:0
4:0
(d)
Zme
Yme
nearside view
(e)
ions (IEA)
ions (IMA)
ions (combined)
electrons (combined)
[cm-3]
n
100
10
1
0.1
0.01
0.001
2:0
3:0
4:0
(f)
2009/ 2/27
[Hz]
f
0.50
0.40
0.30
0.20
0.10
0.00
[nT 2/Hz]
10 1
10 0
10 -1
10 -2
10 -3
(g)
pow > 0.10
polarization
-1 R
0
1 L
(h)
ellipticity
1 circular
0 linear
(i)
θkB
90
80
70
60
50
40
30
20
10
0
(j)
[RL]
Ysse
Xsse
Zsse
1
0
-1
(k)
[nT]
BxSSE
BySSE
BzSSE
10
0
-10

Figure 11.

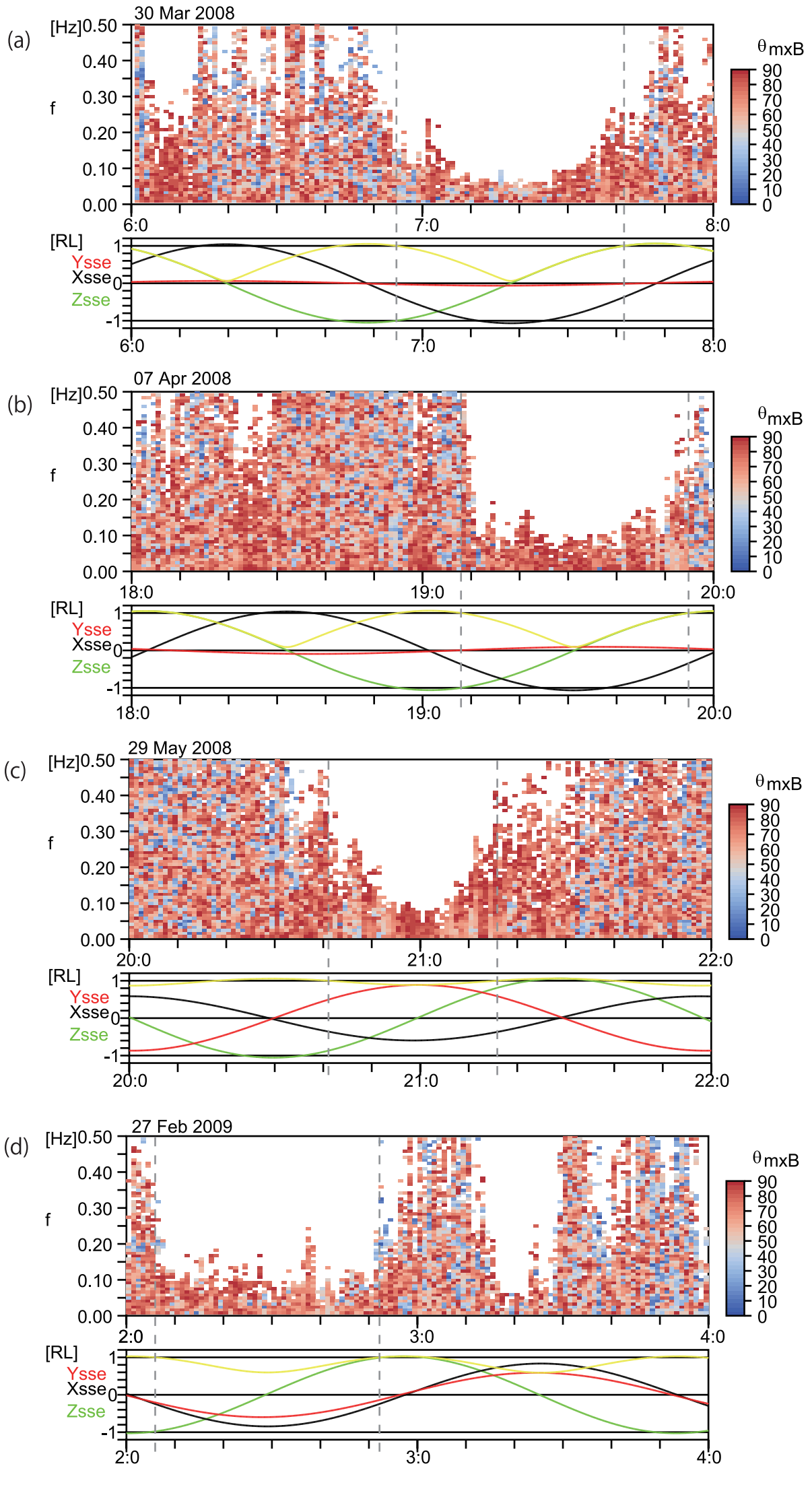
(a)
30 Mar 2008
[Hz]
f
0.50
0.40
0.30
0.20
0.10
0.00
θmxB
90
80
70
60
50
40
30
20
10
0
6:0
7:0
8:0
[RL]
Ysse
Xsse
Zsse
1
0
-1
(b)
07 Apr 2008
18:0
19:0
20:0
(c)
29 May 2008
20:0
21:0
22:0
(d)
27 Feb 2009
2:0
3:0
4:0